Title
STRAIN-CONFINED ELECTRON-HOLE LIQUID IN GERMANIUM

Author
Markiewicz, R.S.

Publication Date
1976-08-01

Published in Physical Review B,
Vol. 15, No. 4, 1988 - 2005
(February 1977)

LBL-6225

STRAIN-CONFINED ELECTRON-HOLE LIQUID IN GERMANIUM

R. S. Markiewicz, J. P. Wolfe, and C. D. Jeffries

August 16, 1976

Prepared for the U. S. Energy Research and
Development Administration under Contract W-7405-ENG-48

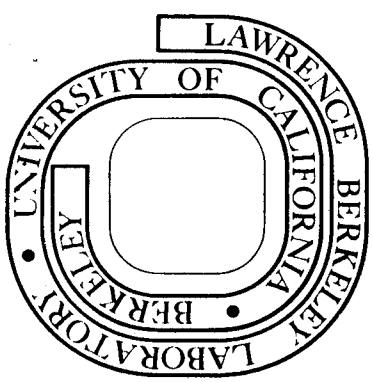

DISCLAIMER

Strain-confined electron-hole liquid in germanium*

R. S. Markiewicz, J. P. Wolfe,† and C. D. Jeffries
Department of Physics, University of California, Berkeley, California 94720
(Received 16 August 1976)

Previous experiments in pure germanium at low temperatures have shown that high densities of photoproduced electron-hole pairs condense into a metallic liquid phase—typically manifested as small electron-hole droplets (EHD). The energy, pair density, and lifetime of an EHD can be significantly modified by applying a stress to the crystal. Due to the lowering of the indirect band edge with strain, droplets, free excitons, and carriers are accelerated in a strain gradient approximately towards a point of maximum shear strain. We show that by appropriately stressing a crystal, it is possible to create inside the crystal a shear strain maximum, i.e., a potential well, into which droplets, excitons, and carriers are attracted, causing them to coalesce into a macroscopic mass of electron-hole liquid with diameter up to a millimeter. Using the known deformation potentials and anisotropies of germanium, we calculate numerically the stress tensor, the band-edge shift, and the electron-hole liquid energy vs position in an inhomogeneously stressed crystal. We report photographic data on large drops in Ge and compare these data to the strain theory. A two-dimensional numerical calculation is in essential agreement with the observed drop locations. Due to the anisotropy of the band-edge shift with strain, we find that it is possible to form one, two, or four electron-hole drops beneath the stress contact area by applying stress along ⟨111⟩, ⟨110⟩, and ⟨100⟩ crystal axes, respectively. In addition we have observed birefringence patterns in these same crystals which yield strain distributions in accord with the above theory and photographic data. Theoretical calculations of the birefringence also agree with observations. Thus the macroscopic features (i.e., position, shape, and number) of the large strain-confined drops can be understood in terms of the known deformation properties of germanium.

I. INTRODUCTION

Since Keldysh's original suggestion[1] of the existence of an electron-hole liquid (EHL) in semiconductors, a variety of experiments have indicated the existence of a metallic liquid phase in germanium at low temperatures.[2] These experiments have shown that high densities of photoproduced electron-hole (e-h) pairs and excitons in Ge can undergo a phase separation into a liquid state. The liquid phase, containing very nearly equal numbers of electrons and holes, is a Fermi fluid displaying the high conductivity of a metal and the surface tension and uniform density of a liquid. Typically, at $T=2$ K in unstressed Ge under continuous illumination, a cloud of small electron-hole droplets (EHD) is formed, each with radius[3,4] 1–5 μm and electron-hole density[5,6] $n \approx 2\times10^{17}$ cm^{-3}. In this paper we show that in suitably stressed Ge, large volumes of the EHL can be produced, with significantly different properties.

In unstressed Ge recombination of e-h pairs in the drop gives rise to a characteristic luminescence[5] at 1.75 μm. The spectrum of the recombination luminescence yields the Fermi energy of the liquid and also the condensation energy ϕ of free excitons onto a drop. From this spectrum the gas-liquid phase diagram of the exciton-EHD system has been studied: the critical temperature is found to be 6.5 K,[7] in reasonable agreement with theory[8–10]; the nature of the drop nucleation process and the surface energy of individual drops has been studied through threshold and hysteresis effects in the EHD luminescence.[11,12]

The stability of the EHL phase is largely attributable to the fact that germanium is an indirect-band-gap semiconductor.[13–15] For unstressed Ge a fourfold degeneracy of the indirect-conduction-band valleys and twofold valence-band degeneracy allows a reduction in kinetic energy for a given density of liquid phase. When the crystal is stressed this degeneracy is partially or wholly removed, leading to a reduced binding energy and reduced equilibrium density n. For the Ge(4 : 2), Ge(1 : 2), and Ge(1 : 1) configurations,[16] Vashishta *et al.*[9,17] have calculated the equilibrium densities of 2.2×10^{17}, 0.69×10^{17}, and 0.11×10^{17} cm^{-3}, respectively. Experimental verification of these latter two values has thus far been difficult. The lowering of the Ge band gap with strain also means that drops, as well as free carriers and excitons, will be attracted toward a region of maximum strain in the crystal. Bagaev *et al.*[18] were the first to observe the lowering of drop energy in strained Ge, and the motion of drops in a strain gradient.

The lifetime τ_d of a droplet in unstressed Ge below 2 K is about 40 μsec, compared to a free-exciton lifetime ~5 μsec. Above 2 K, evaporation of free excitons from the droplet surface greatly decreases the droplet lifetime.[19,20] Consequently, the steady-state volume of electron-hole liquid for a given excitation level is less at high temperatures, and at 4.2 K the luminescence is reduced by perhaps two orders of magnitude. The 40-μsec

lifetime at low temperatures is generally assumed to involve two processes: radiative recombination of an electron and hole, and radiationless Auger recombination involving three or more carriers. If the density n of the liquid phase is decreased by applying a stress to the crystal, then theoretically the recombination rate will decrease proportional to n for the radiative process and to higher powers of n for Auger processes. However, a lengthening of the drop lifetime under "uniform" crystal strains has not been observed; indeed, the opposite has been reported.[6,21] This observed reduction in lifetime for uniaxially stressed crystals could possibly be explained by two factors. First, the condensation energy ϕ is reduced under strain, giving a greatly enhanced evaporation rate, since the thermionic boil-off rate of e-h pairs is proportional to $e^{-\phi/kT}$. This hypothesis would seem to be consistent with the rapid temperature dependence of τ_d observed by Alekseev *et al.*[21] Secondly, a small strain gradient could accelerate droplets to the surface of the crystal, where recombination may be greatly enhanced.[6]

These difficulties can be overcome, however, by choosing a stress geometry which produces a maximum shear stress inside the crystal itself. Such a situation occurs near the contact area of two curved elastic solids. This classic problem in the theory of elasticity was originally solved by Hertz.[22] We find that by applying an appropriate contact stress to a germanium crystal, it is possible to create a potential well into which droplets, excitons, and free carriers are attracted. These coalesce into a large drop of liquid situated near the maximum shear stress region in the crystal. If the drop is not too large (radius $\lesssim 100$ μm), the strain is effectively uniform over the drop volume.

A photograph of a large drop is reproduced in Fig. 1.[23] In this experiment the contact stress is applied to a 4-mm-diam, 1.8-mm-thick disc of Ge by a 1.7-mm-diam nylon set screw. The strain-confined liquid occurs at a point about 0.5 mm inside the crystal and has a radius of 0.3 mm. To obtain this picture the luminescent image of the drop at 1.75 μm was focused onto an infrared-sensitive vidicon, as described later in this paper. Optical excitation was supplied by an 80-mW argon laser beam focused onto the opposite side of the crystal.

The lifetime of this drop is indeed long, measured[24] to be 500 μsec. As previously discussed, the apparent reason for the enhanced lifetime is that the drop is located in a high-stress region where its density is lowered. In addition the effective evaporation rate is greatly reduced by the strain gradient at the surface of the drop: ejected excitons are returned to the liquid in a time short

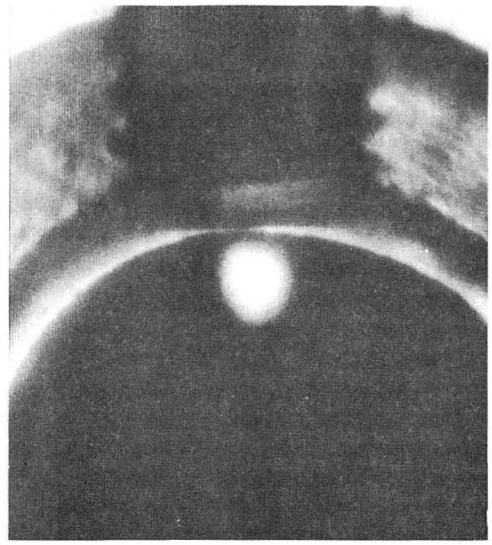

FIG. 1. Photograph of a strain-confined drop of the electron-hole liquid at 2 K in the 4-mm-diam Ge disk, stressed along ⟨110⟩ by a nylon screw (top), and viewed through an (001) face. Central bright region is the e-h recombination luminescence from the liquid confined in a potential well of maximum shear stress, located just below the region of contact. Bright ring around the sample is recombination luminescence scattered from the crystal boundary.

compared with the free-exciton lifetime. In support of this hypothesis, we find experimentally: (i) that the lifetime of a large strain-confined drop is only weakly dependent on temperature up to 4.2 K and (ii) luminescence from excitons in the strain well is observed only at higher temperatures and at low excitation levels. Unlike the droplet phase in unstrained Ge, the EHL luminescence intensity at 4.2 K is about the same as at 2 K, indicating that evaporation from the liquid is greatly inhibited below 4.2 K. Detailed studies of the kinetics and spectroscopy of these large long-lived drops will be reported separately.[25] We find it convenient to label this strain-confined long-lived drop as the γ phase in contrast to the α phase occurring in unstrained Ge. In our experiments, the γ phase corresponds to the lowered configurations, Ge(1 : 2) or Ge(1 : 1), depending on the magnitude of the stress.

Evidence that the luminescent image photographed in Fig. 1 is that of a single drop and not a cloud[26] of small droplets is given by the following experiments: (i) Alfvén wave resonances are observed for this sample consistent with a drop of radius ~0.30 mm and pair density $\sim 10^{17}$ cm^{-3}.[27] The Alfvén wave resonances are standing-wave magnetoplasma modes of the entire drop and require circulating microwave currents throughout

the drop. Resonances at the observed magnetic fields are neither experimentally observed nor theoretically predicted for a cloud of small droplets in an unstressed sample. (ii) The luminescence intensity is much higher from the γ phase than the α phase, corresponding to an average e-h density $\sim 10^2$ times larger than that for clouds ($\sim 10^{15}$ cm^{-3}).[26] (iii) From time-resolved imaging we have found that the radius of the γ drop decays after the light is removed, whereas the α-cloud radius in unstressed Ge does not.[28] (iv) Pokrovskii and Svistunova[29] have recently observed that the Raleigh-Gans light scattering usually associated with small droplets disappears for the long-lived γ phase in stressed Ge. Their absolute measure of the absorption at 3.39 μm corresponded to an e-h density of $\sim 10^{17}$ cm^{-3}—that of a single drop of the liquid phase. Recently, Ohyama, Hansen, and Turney[30] have determined a density of $n = 0.66 \times 10^{17}$ cm^{-3} from magnetoacoustic absorption of a strain-confined drop.

The purpose of this paper is threefold: (i) to present a quantitative theory of the strain-confinement phenomenon for inhomogeneously stressed Ge samples for various geometries used in the experiments; (ii) to report new experimental data on the strain-confined liquid for various stress directions; and (iii) to report theoretical and experimental birefringence studies which determine the strain distribution directly in the Ge samples of interest.

II. BAND-EDGE SHIFTS IN STRAINED GERMANIUM

The lowest-energy conduction-band ellipsoids in germanium are shown in Fig. 2. In unstrained Ge there are four distinct degenerate ellipsoids oriented along the crystalline ⟨111⟩ directions. The addition of a shear strain in this cubic semiconductor reduces the symmetry and changes this band structure. If, for example, a uniaxial stress is applied along one of the ⟨111⟩ axes, the corresponding ellipsoid will shift downward in energy relative to the other three. The valence-band maximum in zero stress consists of one heavy- and one light-hole band degenerate at $k = 0$; this degeneracy is also removed with shear strain. For moderate stresses (~ 10 kg/mm^2) it is possible to split the conduction bands and the valence bands by more than the respective electron and hole Fermi energies in the EHL, thus decreasing the number of populated bands. Figure 3 is a schematic diagram of the various configurations resulting from uniaxial stresses along three symmetry axes.

Since the kinetic, exchange, and correlation energies of e-h pairs within the drop depend upon

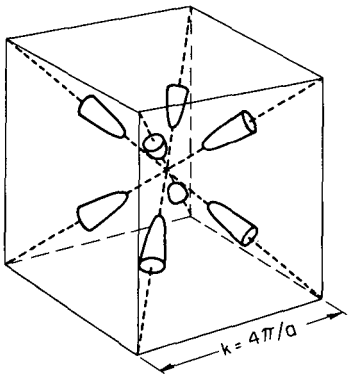

FIG. 2. Lowest conduction-band ellipsoids in Ge, showing the constant energy surfaces $E(k)$ in the first Brillouin zone; the ellipsoids are shown cut at the zone boundary. Edges of the cube shown are parallel to ⟨100⟩ crystal directions. Lattice constant $a = 5.65$ Å for Ge.

the degeneracy of the bands, it is expected that the equilibrium density, binding energy, critical temperature, and other drop parameters will be strongly dependent on strain. Vashishta *et al.*[9,17] have calculated EHL parameters for the Ge(4:2), Ge(1:2), and Ge(1:1) configurations. Even in the Ge(1:1) case they find that the liquid phase is still slightly bound with respect to free excitons and that the density is greatly reduced to $n \simeq 0.11 \times 10^{17}$ cm^{-3}. The reduction in binding energy and density occurs primarily because the kinetic-energy term is much larger for nondegenerate bands.[13-15]

To describe the shift of the band edge with strain in Ge, we define the usual second-rank strain tensor, a typical component being

$$\epsilon_{xy} = \frac{1}{2}\left(\frac{\partial u_x}{\partial y} + \frac{\partial u_y}{\partial x}\right), \tag{1a}$$

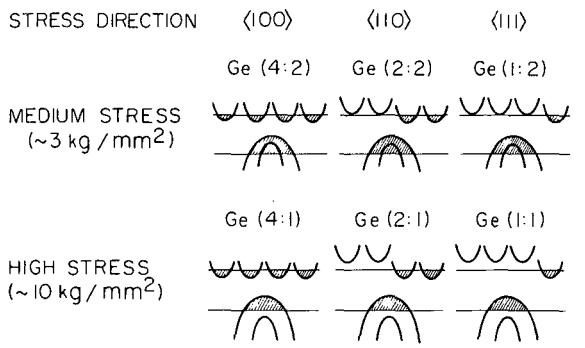

FIG. 3. Splitting of the electron and the hole bands in Ge under uniaxial compression. For example, stress along a ⟨111⟩ direction lowers one electron ellipsoid in energy relative to the other three. For a medium stress this splitting exceeds the Fermi energy of the electrons, and only one ellipsoid is populated; since both hole bands are still populated, we denote this configuration as Ge(1:2). At higher stresses only one hole band is populated, denoted by Ge(1:1). Unstressed Ge is denoted by Ge(4:2).

where u_x is the local displacement in the x direction. For the inhomogeneous strains of interest in this paper the elements of this tensor are functions of position in the crystal. The local stress tensor $\vec{\sigma}$ is related to $\vec{\epsilon}$ through the stiffness tensor $\underline{C}$:

$$\vec{\sigma} = \underline{C} : \vec{\epsilon} . \tag{1b}$$

The shift of the ith conduction band with strain is described in terms of the deformation potentials Ξ_u and Ξ_d introduced by Herring and Vogt,[31]

$$\Delta E_c^i = \Xi_u \hat{a}_i \cdot \vec{\epsilon} \cdot \hat{a}_i + \Xi_d \, \mathrm{Tr}\vec{\epsilon} , \tag{2}$$

where a_i is the unit vector pointing along the ith valley (i.e., a $\langle 111 \rangle$ direction) and $\mathrm{Tr}\vec{\epsilon} = \epsilon_{xx} + \epsilon_{yy} + \epsilon_{zz}$. This may be written in the form

$$\Delta E_c^i = \Delta E_c^{\mathrm{mean}} + \Xi_u \epsilon_0^i , \tag{3a}$$

where

$$\Delta E_c^{\mathrm{mean}} = (\Xi_d + \tfrac{1}{3}\Xi_u)\,\mathrm{Tr}\vec{\epsilon} \tag{3b}$$

is the average shift of all four conduction bands, and ϵ_0^i, which determines the relative shift of the ith band, is defined by

$$\epsilon_0^i = \hat{a}_i \cdot \vec{\epsilon} \cdot \hat{a}_i - \tfrac{1}{3}\,\mathrm{Tr}\vec{\epsilon} . \tag{3c}$$

The shear strains ϵ_0^i will be shown to have a dominant influence on the band gap shift, and some of their properties are described in the appendix.

The shift of the jth valence-band edge is

$$\Delta E_v^j = a\,\mathrm{Tr}\vec{\epsilon} + (-1)^j |E_{\epsilon\epsilon}| , \tag{4a}$$

$$E_{\epsilon\epsilon}^2 = \tfrac{1}{2}b^2[(\epsilon_{11} - \epsilon_{22})^2 + \text{c.p.}] + d^2(\epsilon_{12}^2 + \text{c.p.}) , \tag{4b}$$

where a, b, and d are the hole deformation potentials of Picus and Bir[32] and c.p. stands for cyclic permutation with respect to 1, 2, and 3. The indices 1, 2, 3 refer to the $\langle 100 \rangle$ axes of the crystal; x, y, z axes will be defined later with respect to the applied stress direction and crystal face. The electron and hole deformation potentials were determined by Balslev[33] by analyzing the shift in the indirect absorption edge with uniaxial stress. His average values for Ge at 80 K are listed in Table I. The strain-split band edges give rise to a number of band gaps: $E_g^{ij} = E_g(\epsilon = 0) + \Delta E_c^i - \Delta E_v^j$. Carriers relax toward the minimum band gap:

$$E_g(\epsilon) = \min_{ij}(E_g^{ij}) = E_g(0) + (\Xi_d + \tfrac{1}{3}\Xi_u - a)\,\mathrm{Tr}\vec{\epsilon} - |E_{\epsilon\epsilon}| - \Xi_u[\max_i(-\epsilon_0^i)] . \tag{5}$$

In Fig. 4(a) the resulting shift ΔE_g of the minimum band gap versus uniaxial stress is plotted for three crystal directions.

From the magnitudes of the deformation potentials listed in Table I, it is apparent that the primary source of the band-gap shift is the last term of Eq. (5) due to the conduction-band splitting.

TABLE I. Values of Ge deformation potentials measured at $T = 80$ K by Balslev, Ref. 33.

Ξ_u	16.2 ± 0.4 eV
b	-1.8 ± 0.3 eV
d	-3.7 ± 0.4 eV
$\Xi_d + \frac{1}{3}\Xi_u - a$	-2 ± 0.5 eV

We define the octahedral shear strain as

$$\epsilon_0^m = \max_i(-\epsilon_0^i) . \tag{6}$$

If the strain is not uniform, then, the free-carrier energy will be a function of position, and will minimize approximately at the point of maximum octahedral shear strain, ϵ_0^m. (Since compressional strains are taken as negative, ϵ_0^m is greater than zero.) Since the corresponding octahedral shear stress σ_0^m is linearly proportional to ϵ_0^m (Appendix), we may also say that free carriers are attracted to regions of maximum octahedral shear stress.

The shift of the EHD peak luminescence energy with uniaxial stress has been determined experimentally.[6,18,21] The data of Benoit *et al.*[6] are

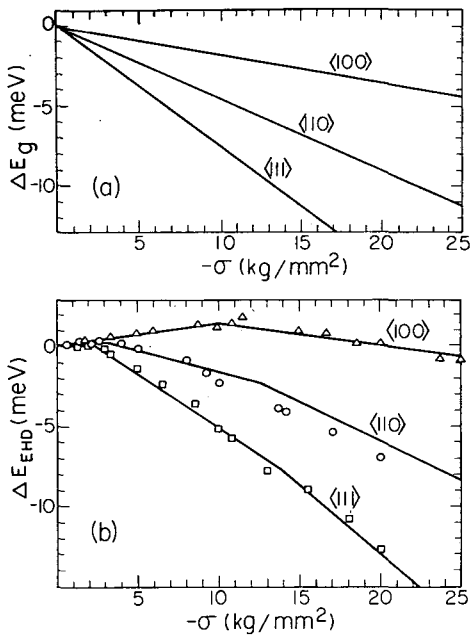

FIG. 4. (a) Shift in band-gap energy with uniaxial stress at 80 K in Ge: $\Delta E_g = E_g(\epsilon) - E_g(0)$ from Eq. (5). Lines drawn have slopes corresponding to the data of Balslev (Ref. 33). We employ the convention that compressional strains and stresses are negative. (b) Shift of EHL energy with uniaxial stress: $\Delta E_{\mathrm{EHL}} = E_{\mathrm{EHL}}(\epsilon) - E_{\mathrm{EHL}}(0)$. Data points are taken from Benoit *et al.* (Ref. 6). Solid lines show the energy shift calculated from Eqs. (7) and (1b).

plotted in Fig. 4(b). It is apparent that the energy of an EHD does not follow the band-edge shifts in the lower stress regions. For the ⟨110⟩ and ⟨111⟩ directions, the initial increase in the drop energy with stress is due to the decrease in EHL binding energy as the conduction-band degeneracy is reduced. The positive initial slope for a ⟨100⟩ stress was interpreted as a change in binding energy as the valence-band degeneracy is removed. Once the strain-split bands are completely depopulated, the drop energy shift is approximately parallel to the band-gap shift. At these stresses the exciton shift is also parallel to the band-gap shift.[33] Thus carriers, excitons, and droplets will be attracted to regions of maximum octahedral shear stress.

We obtain an empirical expression for the EHL binding energy E_B as a function of stress by assuming: (i) that each populated conduction or valence band contributes additively to the total E_B; and (ii) that the contribution from each band decreases proportionally to the strain-induced splitting, until the point at which that band is completely depopulated. Thus the e-h pair energy in the drop is

$$E_{\mathrm{EHL}}(\epsilon) = E_g(\epsilon) - E_B(\epsilon), \tag{7}$$

where $E_g(\epsilon)$ is defined in Eq. (5), and

$$E_B(\epsilon) = E_B(0) - \alpha_v \delta E_v - \alpha_c \sum_i \delta E_c^i, \tag{8}$$

$$\delta E_v = \begin{cases} 2|E_{\epsilon\epsilon}| & \text{if } 2|E_{\epsilon\epsilon}| < E_{v0}, \\ E_{v0} & \text{if } 2|E_{\epsilon\epsilon}| \geq E_{v0}, \end{cases} \tag{9}$$

$$\delta E_c^i = \begin{cases} \Delta E_c^i - \Delta E_c^{\min} & \text{if } \Delta E_c^i - \Delta E_c^{\min} < E_{c0}, \\ E_{c0} & \text{if } \Delta E_c^i - \Delta E_c^{\min} \geq E_{c0}. \end{cases} \tag{10}$$

We have fit the uniaxial stress data of Benoit *et al.* to Eq. (7) and obtain the parameters $\alpha_v = 1.24$; $\alpha_c = 0.21$; $E_{v0} = 2.23$ meV, and $E_{c0} = 2.43$ meV. The result is shown as the solid lines in Fig. 4(b). Equation (7) allows us to estimate the drop energy shift produced by stressing the crystal in an arbitrary direction.

III. HERTZ CONTACT PROBLEM

The problem of the distribution of strains produced when two elastic solids press against each other was first solved by Hertz,[22,34] who originally considered the contact region between two solids with ellipsoidal surfaces. The area of contact produced between the two curved surfaces is a function of the applied force and the elastic properties of the solids. One consequence of Hertz's solution is that the maximum shear strain occurs not *at* the contact surface but in the *interior* of the solids.[35]

An explanation of this phenomenon is given in Fig. 5, which represents the numerically calculated shear stress components of a germanium sample stressed along ⟨110⟩ by a nylon rod,[36] as discussed in Sec. IV. We consider a two-dimensional problem where z is the coordinate along the applied force direction into the solid and y is the coordinate perpendicular to this force; $z = 0$ is at the contact surface. The compressional stresses along these axes, σ_{zz} and σ_{yy}, are plotted in Fig. 5 as a function of z along the force axis, $y = 0$. The lateral stress σ_{yy}, while large at the surface of contact, falls off much more rapidly with distance than the longitudinal component, σ_{zz}. Thus the component of shear stress $\tau = \sigma_{zz} - \sigma_{yy}$ has a maximum inside the solid. This result comes about because at large distances from the contact surface the stress pattern will not be sensitive to the exact stress distribution on that surface but will respond as if there were a uniform uniaxial stress on the surface. That is, σ_{zz} will be approximately constant and $\sigma_{yy} \approx 0$.[37] Very near the contact surface, however, σ_{yy} can be large.

In the above case the maximum calculated value of τ occurs at a distance $r_0 \approx 0.75a$ from the surface, and has a magnitude $\tau_0 \approx 0.9F/A$, where F is the applied force, a is an average radial extent of the contact area, and A is the contact area. (For a two-dimensional calculation, F/A is actually $F'/2a$, where F' is the force per unit thickness of the crystal in the third dimension, and $2a$ is the

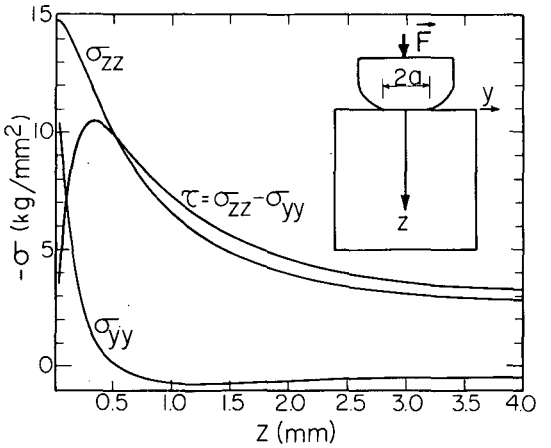

FIG. 5. Variation of compressional stress components σ_{zz} and σ_{yy}, and shear stress, $\tau \equiv \sigma_{zz} - \sigma_{yy}$, with position inside a Ge crystal stressed along ⟨110⟩ as shown in the insert. Note that for this geometry the shear stress τ has a maximum inside the crystal; this forms a potential well for the e-h liquid. Actual elastic constants of Ge and nylon are used in this and subsequent calculations (Ref. 36).

width of the contact region.) These values for r_0/a and $\tau_0/(F/A)$ are close to those usually found in contact problems involving isotropic solids.[34]

IV. NUMERICAL SOLUTIONS FOR THE STRAIN DISTRIBUTION: TWO-DIMENSIONAL MODEL

In this section we consider the problem of the strain distribution produced by pressing a nylon rod against a Ge crystal. Since Hertz's analytic solution to the contact problem applies to isotropic elastic solids where the deformation is small compared to the size of the body, it is not directly applicable to the present problem, because of the anisotropic elastic properties of Ge and the relatively large deformation of the nylon. Thus the strain distribution in the sample has been calculated numerically. Both sample and nylon rod have been represented by finite arrays of volume elements, and the differential equations of elasticity have been replaced by a finite set of equations coupling the elements. This set of equations was then solved numerically, using standard finite element techniques.[38] Figure 6 shows the grids of elements used to represent the materials, for both square and cylindrical cross sections. The computer program calculates all components of the stress and strain tensors at a point inside each volume element of the crystal. From the resulting strain tensor the local band-edge shift and EHL energy can be calculated using Eqs. (5) and (7).

Some approximations are required to reduce the actual problem to a form tractable for calculations. First, the sample is treated as two dimensional[39] by ignoring the variation of strain in the third dimension. An approximate three-dimensional strain distribution may be obtained by making two-dimensional calculations along two pairs of axes at right angles to each other, as will be described in Sec. V. Further approximation is necessary to describe the contact between the nylon and the Ge. In the actual experiments, the stress was initially applied at room temperature, where the nylon was softer and more plastic, so that a large, smooth contact area was formed. When the plastic cooled down this deformation was frozen in, so that large variations in the applied force produced little change in the contact area. In our computations we calculated the deformations using the room-temperature elastic constants of nylon and Ge and assumed that at low temperatures this strain pattern is frozen in. In the calculations for the square Ge sample (Fig. 6), the radius of curvature R of the nylon plunger was varied in order to fit the calculated position of the EHL potential minimum to the observed position; the best fit was found for $R = 20$ mm, which is larger than the initial radius of curvature, because of plastic deformation of the nylon. It was found that, for a fixed area of contact, the strain pattern, and consequently the band-gap energy shift, scaled linearly with the applied force F. Furthermore, the diameter of the contact area was proportional to $(FR/Y)^{1/3}$, where Y is the Young's modulus of the nylon. In principle, the strain pattern can depend on the transverse frictional contact between the nylon and the Ge; in our computations, we found almost identical strain patterns for the two extreme cases of free sliding and perfect sticking contacts between Ge and nylon. The former case is assumed in all the figures shown. To summarize, we feel that the most severe approximations are the two-dimensional nature of the calculation and our simple model of the drop binding-energy shift with stress, Eq. (8).

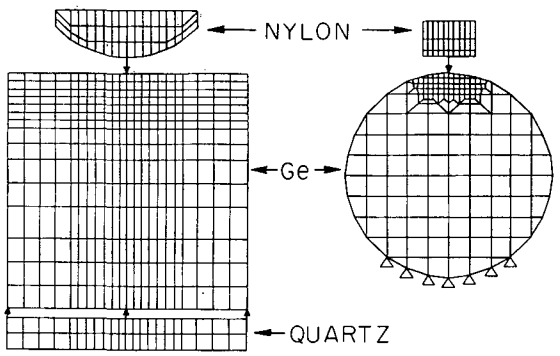

FIG. 6. Grids of elements used to represent the Ge crystal and the nylon rod in the finite element analysis. For the square-cross-section sample, the Ge was seated on a slab of fused silica, as in the actual experiment. In the experiments with cylindical samples, the Ge was seated in a cylindrical plastic holder; the calculation was simplified by rigidly fixing the set of grid points shown.

Figure 7 shows the results of a finite element calculation for a square solid with isotropic elastic properties, giving the spatial distributions of two different shear strain components: $\epsilon_{yy} - \epsilon_{zz}$ in Fig. 7(a) and ϵ_{yz} in Fig. 7(b). The strain component $\epsilon_{yy} - \epsilon_{zz}$ is proportional to the corresponding shear stress τ, described in Sec. III: the maximum strain occurs inside the crystal, along the axis on which the applied force is centered. The strain component ϵ_{yz} behaves in a quite different manner. This strain vanishes along the applied force axis by symmetry, so that there must be two strain maxima, one on either side of this axis.

Figure 8 shows the strain components calculated using the anisotropic stiffness tensor of Ge. By comparison to Fig. 7 we conclude that the elastic anisotropy does not significantly alter the distribution of strains. However, the resulting band-gap shift, Fig. 9, does depend sensitively on the orien-

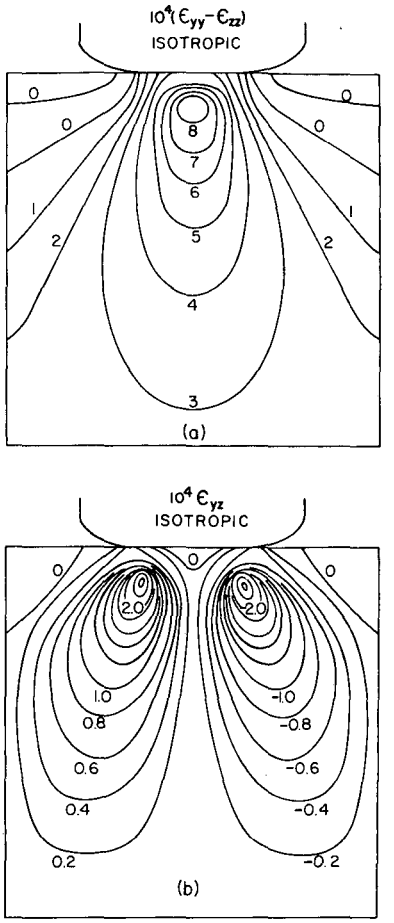

FIG. 7. Calculated shear strain components in "isotropic Ge." For this calculation the cubic stiffness tensor of Ge was replaced by isotropic values of comparable magnitude derived from Young's modulus $Y = 1.39 \times 10^{12}$ dyn/cm^2, Poisson's ratio $\nu = 0.3$. Curves indicate lines of constant strain.

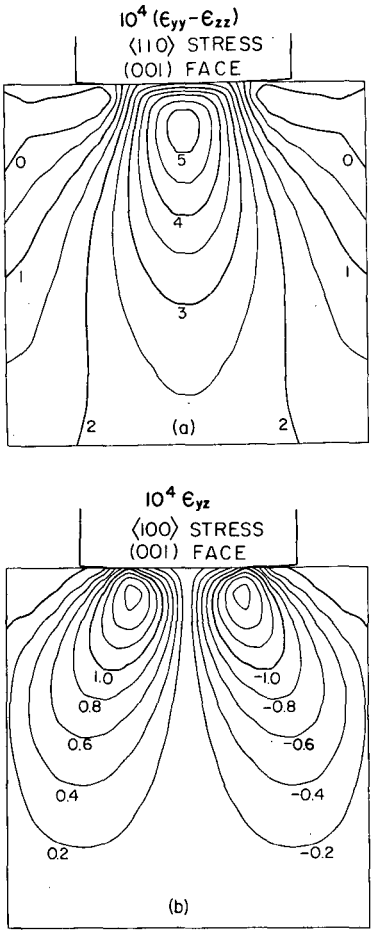

FIG. 8. Calculated shear strain components in Ge. This figure shows the octahedral shear strain distribution [Eq. (6)] produced in two different stress geometries for a crystal of 4-mm width. The width of the region of contact is $2a = 1.4$ mm, and the total force per unit thickness applied across the interface is 10 kg/mm.

tation of the crystal axes with respect to the direction in which pressure is applied, since the shift depends primarily on the octahedral shear strain [Eq. (6) and the Appendix]. For a two-dimensional crystal with viewing face perpendicular to an ⟨001⟩ axis (x direction), the octahedral shear strain ϵ_0^m is proportional to ϵ_{yz} if the force direction (z axis) is along a ⟨100⟩ direction, whereas $\epsilon_0^m \propto (\epsilon_{yy} - \epsilon_{zz})$ if the z axis is along a ⟨110⟩ direction [Eqs. (A3), (A4)]. Thus in the latter example [Fig. 8(a)], there will be a single band-gap minimum in the crystal, whereas in the former case [Fig. 8(b)] there will be two minima visible in two dimensions. The physical interpretation of this difference will be discussed in Sec. V, which will generalize these results to three dimensions. Figure 9 shows the band-gap shift distributions in these crystals, calculated by substituting the strain distributions found previously (Fig. 8) into Eq. (5).

Finally, using these same strain distributions and Eq. (7), the energy of the EHL in the strained crystals is calculated and plotted in Fig. 10. As expected, the results are similar to the distributions of octahedral shear strain (Fig. 8) and band-gap shift (Fig. 9). We find that general features of the results (e.g., number of minima) do not depend sensitively on the shape of the crystal: Figure 11 displays the band-gap shift calculated for a sample with cylindrical cross section. This is the geometry used in Figs. 1 and 19–21. The calculations have also been carried out for stress applied in other directions: Figure 12 shows the band gap and EHL energy shifts for a crystal stressed along a ⟨111⟩ direction and viewed through a $(1\bar{1}0)$ face. A single-energy minimum is produced.

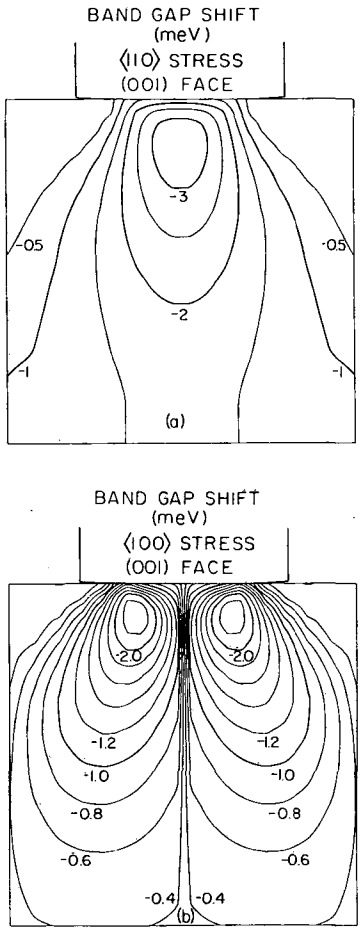

FIG. 9. Calculated band-gap shift ΔE_g in stressed Ge (in meV). These results are obtained by using Eq. (5), and the total strain distribution calculated for the example of Fig. 8.

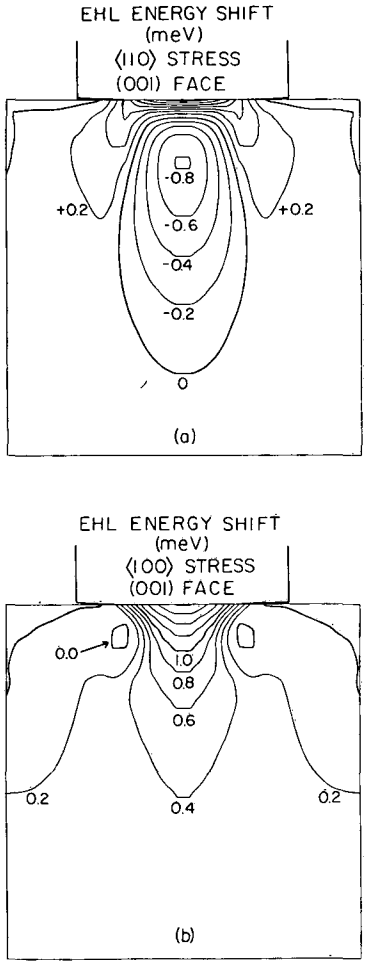

FIG. 10. Calculated EHL energy shift ΔE_{EHL} in stressed Ge (in meV). These results are obtained by using Eq. (7) and the total strain distribution calculated for the sample of Fig. 8.

The energy minima are three-dimensional potential wells in which large, single drops of EHL can form. Figure 13 displays the variation of energy with position inside the crystal along two perpendicular axes passing (approximately) through the center of the well; the curves shown are for the geometry of Fig. 12. The variation of energy with y is well represented by a parabola:

$$\Delta E = -E_0 + \beta(y - y_0)^2 . \tag{11a}$$

The solid curves in Fig. 13(b) are given by Eq. (11a), using the parameters: ΔE_{EHL}: $E_0 = 3.3$ meV $y_0 \approx 10^{-4}$ mm, $\beta = 7.9$ meV/mm^2 ΔE_g: $E_0 = 6.3$ meV, $y_0 = 7\times10^{-3}$ mm, $\beta = 8.3$ meV/mm^2. The variation of energy with z is found to be fit approximately by

$$\Delta E = E_1 - B_1/z' + B_2/(z')^5 , \tag{11b}$$

$$z' = z + z_1 , \tag{11c}$$

which is represented as the solid curves in Fig. 13(a), with the parameters: ΔE_{EHL}: $E_1 = 2.1$ meV, $z_1 = 1.2$ mm, $B_1 = 10.5$ meV mm, $B_2 = 13$ meV mm^5; ΔE_g: $E_1 = 1.0$ meV, $z_1 = 1.3$ mm, $B_1 = 15$ meV mm, $B_2 = 21$ meV mm^5. The term in $(z')^5$ was chosen merely to give the best fit, but the strains, and therefore ΔE_g, are expected to fall off as z^{-1} for large z, in a two-dimensional model—see Sec. V, especially Ref. 41. For a drop of $r \leq 200$ μm formed in such a well, the energy ΔE_{EHL} varies by $<10\%$ over the drop volume. Thus although the strain distribution is highly nonuniform through the crystal as a whole, it is approximately constant near the potential minimum. It must be kept in mind that these calculations are made for a two-dimensional model and the numerical results are only approximately applicable in the actual three-dimensional case.

Once the strain distribution is known, the re-

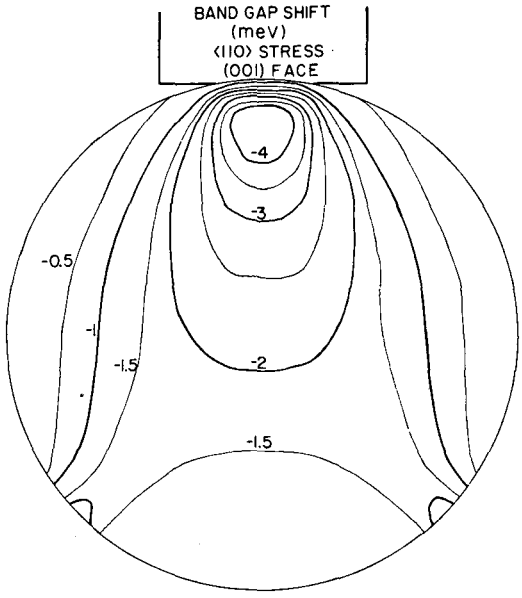

FIG. 11. Band-gap shift (in meV) in a stressed, cylindrical Ge sample. These results are obtained in an analogous manner to the results shown in Fig. 9(a). Applied force per unit thickness is 10 kg/mm and the contact width is $2a = 0.9$ mm (disk diameter = 4 mm).

sulting strain-induced birefringence can also be calculated. The difference in refractive index along and perpendicular to the stress-induced optic axis can be related to the strain tensor through the strain-optic tensor $\underline{p}$.[40] For the geometries corresponding to Figs. 8–10 [an (001)-face crystal], we find

$$\Delta n = \tfrac{1}{2}\kappa_L^{3/2}[(p_{11}-p_{12})^2(\epsilon_{zz}-\epsilon_{yy})^2 + 4p_{44}^2\epsilon_{yz}^2]^{1/2}$$
$$\simeq \kappa_L^{3/2} p_{44}|\epsilon_{yz}| = \tfrac{3}{2}\kappa_L^{3/2} p_{44}\epsilon_0^m , \qquad (12)$$

for stress along ⟨100⟩. For stress along ⟨110⟩:

$$\Delta n = \tfrac{1}{2}\kappa_L^{3/2}[p_{44}^2(\epsilon_{zz}-\epsilon_{yy})^2 + 4(p_{11}-p_{12})^2\epsilon_{yz}^2]^{1/2}$$
$$\simeq \tfrac{1}{2}\kappa_L^{3/2} p_{44}(\epsilon_{yy}-\epsilon_{zz}) = \tfrac{3}{2}\kappa_L^{3/2} p_{44}\epsilon_0^m , \qquad (13)$$

where κ_L is the dielectric constant of Ge. The approximate expressions hold for Ge since $|p_{44}| = 0.078 \gg |p_{11}-p_{12}| \simeq 0.01$. The intensity pattern of light transmitted through a crystal placed between crossed polarizers at ±45° to the optic axis is proportional to $\sin^2(2\pi N)$, where N is given by

$$N = d\Delta n/\lambda , \qquad (14)$$

where d is the crystal thickness and λ is the wavelength of light used. Figure 14 shows the fringe order N calculated using the full expressions for Δn and the previously calculated strain distributions. The birefringence shows a maximum stress at approximately the same position in the crystal as the minimum of EHL energy. This can be understood from the approximate form of Eqs. (12) and (13), which show that Δn is proportional to the octahedral shear strain. In the appendix, we show that this result holds for stresses along an arbitrary direction.

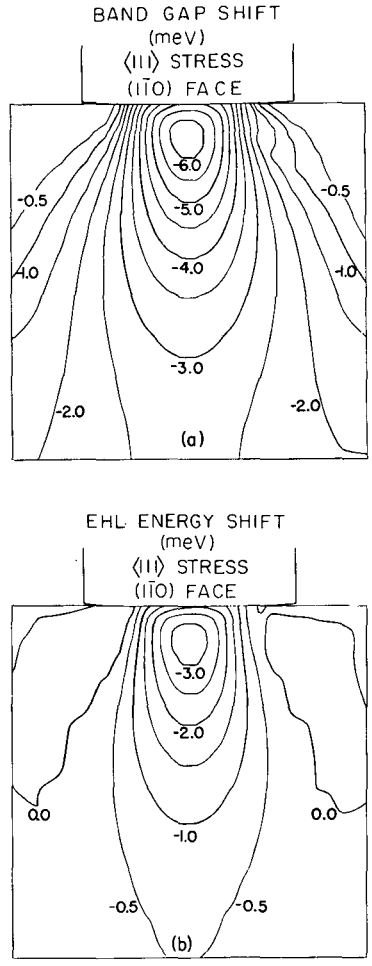

FIG. 12. Band-gap and EHL-energy shift (in meV) in stressed Ge. Calculations were made as in Figs. 9 and 10, with $F' = 10$ kg/mm and $2a = 1.4$ mm but now with the force applied along a ⟨111⟩ axis, and the crystal face taken as (110).

V. EXTENSION TO THREE DIMENSIONS

We have not attempted to extend the finite element calculation of the strain distribution to a three-dimensional model of Ge. However, an indication of the resulting strain distribution can be obtained from the two-dimensional strain calculations for two mutually perpendicular cross sections of the crystal. For example, Fig. 15 again shows the drop energy distribution calculated assuming the force is applied along a ⟨110⟩ direction, but the crystal is now viewed through a

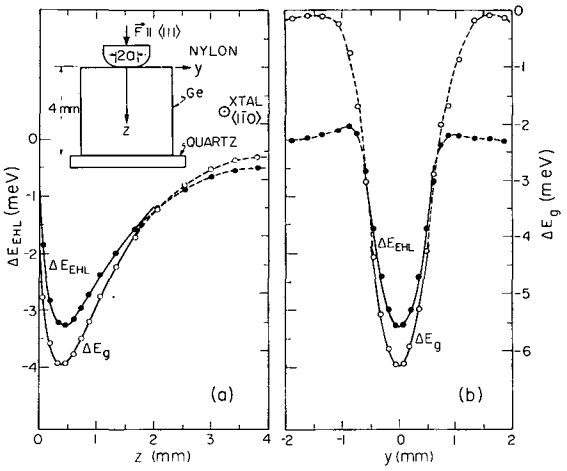

FIG. 13. Variation of band-gap (○) and EHL (●) energy with position inside a square Ge crystal, stressed along ⟨111⟩ as shown in the insert. Dashed lines are smooth curves connecting the theoretical points, taken from the calculations represented by Fig. 12. (a) Variation of energies in the direction of applied force (z-axis). Solid lines represent Eq. (11b), an analytical approximation to the calculated points. (b) Variation of energies along the y axis through the well minima. Solid lines are plots of Eq. 11(a). The slight asymmetry in y is because Ge is not symmetric under reflection in a (112) plane [see Fig. 23(c)].

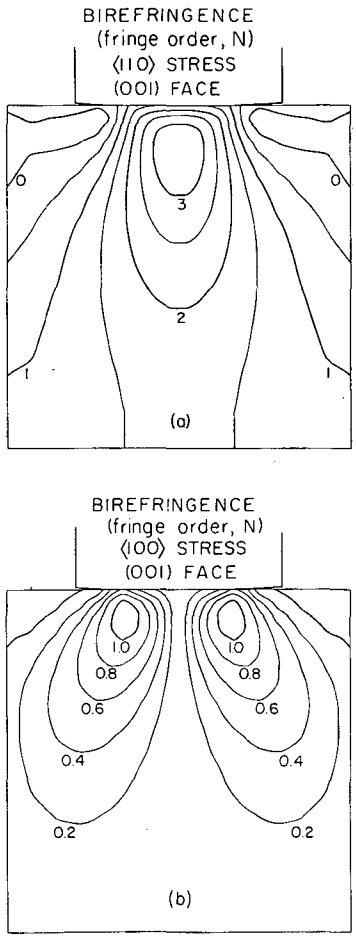

FIG. 14. Fringe order N [Eq. (14)] in stressed Ge. Observed birefringence pattern is given by $\sin^2(2\pi N)$. Strain distribution used is the same as in Figs. 8–10, and the fringes are calculated using the full Eqs. (12) and (13), and assuming a crystal thickness $d = 2$ mm and $\lambda = 1.7$ μm. For stress applied along a ⟨110⟩ [Fig. 14(a)] the pattern occurs when the axes of polarization are at ±45° to the applied force direction, whereas for stress along ⟨100⟩ [Fig. 14(b)], the polarization axes must be along and perpendicular to the force direction in order to observe any birefringence pattern.

(1$\bar{1}$0) face, at right angles to the crystal shown in Fig. 10(a). It is evident that two minima are formed in this case, and that in the Fig. 10(a) view one minimum obscures the other. Note that the potential wells are much deeper in Fig. 15 than in Figs. 9(a) and 10(a). This occurs because the two-dimensional calculation of Figs. 9 and 10 is representative of strains in the center plane of the crystal, which does not pass through the energy minima. For the case of a stress applied along an ⟨001⟩ axis [Fig. 10(b)], a 90° rotation of the crystal about this axis will bring the crystal back to another (100) face, so that two minima will again be observed. Thus we find that four energy minima are formed in the real three-dimensional crystal when the force is applied along an ⟨001⟩ direction.

The number of minima produced, as well as their relative positions inside the crystal, can be understood on the basis of a simple physical argument. The basic observation, Fig. 4, is that a stress along a ⟨111⟩ axis can produce a larger EHL energy lowering than an even greater stress along any other axis. Since, in our experiments, the stress distribution is highly inhomogeneous, there is always at least one point in the crystal where the stress tensor will have the form of a ⟨111⟩ uniaxial stress; if the magnitude of this stress is large enough, the drop energy will minimize near these points rather than directly along the applied force direction.

To make this idea more quantitative we must estimate (a) where in the crystal these ⟨111⟩ stresses occur, and (b) how their magnitudes compare with the magnitude of the stress along the applied force axis. We consider a special model in which the plunger and Ge make contact at only a single point. For an isotropic elastic tensor the resulting stress distribution is known[41]: the stress at any point in the crystal is approximately a uniaxial compression directed radially away from the point of contact (Fig. 16 inset). In three di-

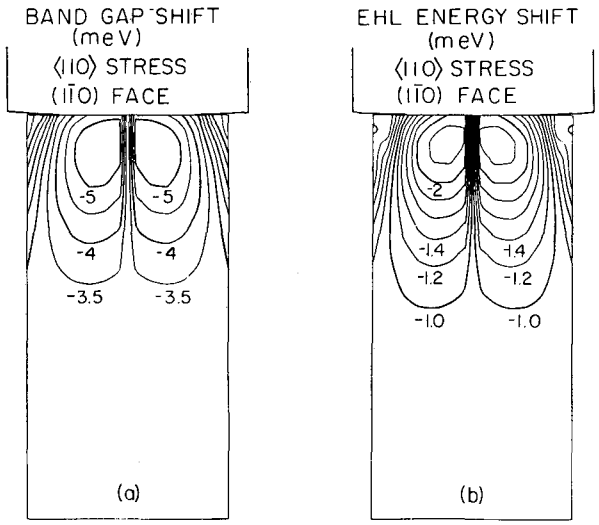

FIG. 15. Band-edge and EHL energy shifts (in meV) in stressed Ge [force along ⟨110⟩, (1$\bar{1}$0) face]. This calculation represents a cross section of Ge cut at right angles to that of Figs. 9(a) and 10(a). The thickness of the crystal is 2 mm.

mensions the magnitude of the stress is proportional to $r^{-2}\cos\theta$, where r is the radial distance from the point of contact and θ is the angle between the radius vector and the direction of applied force. This simple model is not applicable too near the point of contact, where the stresses become infinite; however, at large enough radial distances r, it should give a reasonable estimate of how the stresses vary with θ.

Since we have shown that the anisotropy of the elastic tensor in Ge does not greatly alter the stress distribution, we consider this stress distribution to be approximately valid in Ge. If the force is applied along a ⟨110⟩ axis, there is a ⟨111⟩ axis at $\theta = 35.3°$ from this direction. The respective stresses will be σ_m and $\sigma_m \cos\theta$ along ⟨110⟩ and ⟨111⟩. In Fig. 16, we show that the band-gap energy lowering is greater along the ⟨111⟩ axis than along ⟨110⟩, even though the stress is smaller along ⟨111⟩. By symmetry there will be two minima in this geometry.

Thus *the energy minima will occur not on the force axis but more nearly along the ⟨111⟩ axes nearest it.* A similar analysis to the above confirms that there should be four EHL energy minima formed by stressing Ge in a ⟨100⟩ direction, whereas stress directly along a ⟨111⟩ axis will produce a single minimum along the force axis. These results agree with the two-dimensional calculations described above, and will be confirmed experimentally in Sec. VII.

We note that when the EHL energy is lowered by ⟨111⟩ uniaxial stress [Fig. 4(b)], then the only electron ellipsoid which is populated is the one along the corresponding ⟨111⟩ axis in momentum space. Thus the EHL produced at these stress maxima will be in the configuration Ge(1 : 2) or Ge(1 : 1), Fig. 3, depending on the magnitude of the stress.

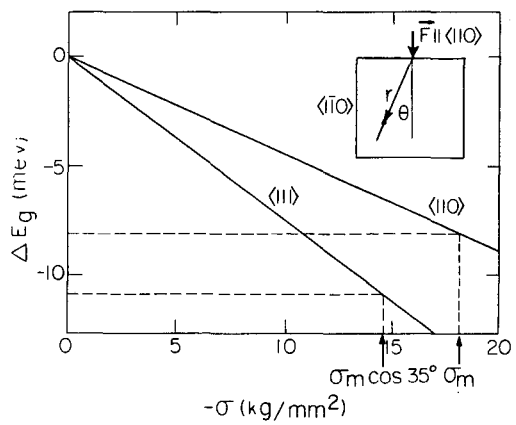

FIG. 16. Method of locating the point of minimum band gap in a three-dimensional crystal. The insert shows the stress geometry assumed: force along ⟨110⟩ and viewing face (1$\bar{1}$0). See text for an explanation of σ_m.

VI. EXPERIMENTAL PROCEDURE

The germanium crystals used in these experiments were cut from an ultrapure dislocation-free boule of p-Ge containing $N_A \lesssim 10^{11}$ cm^{-3} grown by Hansen and Haller.[42] Oriented disks 4-mm-diam $\times$1.7-mm-thick and squares $4\times4\times2$ mm^3 were etched with either CP4 solution (HF:acetic acid : HNO_3 : Br in the ratios 50 : 50 : 80 : 1) or $3HNO_3$: 1HF solution. The crystals were mounted and stressed as shown in Fig. 17. The contact stress was applied to the sample by means of a nylon rod. This plunger was often simply a 1-72 nylon screw, cut off flat for the disk samples or rounded slightly ($R \sim 4$ mm) for square samples. The slight curva-

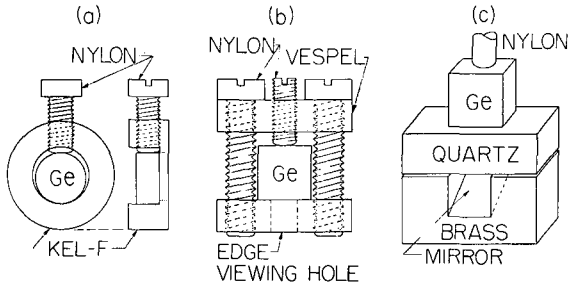

FIG. 17. Experimental arrangements for applying inhomogeneous stress to Ge samples. (a) and (b), "permanent stress" holder; (c) variable stress apparatus.

ture of at least one of the contact surfaces (crystal or plunger) is necessary to produce a shear stress maximum inside the crystal, Sec. III. Care must be taken to avoid surface roughness or sharp discontinuities in the region of contact. A raised point on the contact surface can be described as forming a contact with very small contact area but large applied force. Consequently, the shear strain maximum will be large and very near the crystal surface. A distribution of these microstrains will attract the EHD to the crystal surface and prevent the formation of large drops. We have avoided these problems by making the contact with a soft plastic rod or by inserting a thin sheet of mylar between the sample and the rod.

In the dielectric (KEL-F) holder of Fig. 17(a) the screw is lightly tightened against the Ge sample at room temperature, and the assembly cooled down. The shrinkage of the KEL-F consistently produced a contact force of ~10 kg, as determined by birefringence measurements. This "permanent-stress" holder was adaptable to the microwave Alfvén resonance experiments previously reported; once mounted the sample displayed reproducible large drops for an indefinite number of temperature cycles. A "permanent stress" plastic holder which was equally successful for square samples is shown in Fig. 17(b).[43] A hole in the bottom allowed viewing along the stress direction. An apparatus providing variable stress *in situ* is shown in Fig. 17(c). The force on the nylon contact plunger is transmitted by a stainless-steel rod from a calibrated spring arrangement exterior to the cryostat. The Ge crystal is placed on a transparent quartz plate, beneath which is a 45° mirror, permitting optical viewing along the stress direction. Stresses from 0–25 kg/mm^2 have been applied to the Ge with this apparatus. A modification of this geometry was used for stressing disk samples. Typically a 10-kg force is applied by the plunger before cooldown.

The experimental arrangement for photographing an electron-hole drop is shown in Fig. 18(a). The output of a 2-W Ar-ion laser is filtered with a H_2O bath to attenuate the infrared output of the plasma tube. The laser beam is focused through three quartz windows onto the Ge crystal immersed in liquid He in a ^{4}He cryostat; typical spot size was ~100-μm diameter. The image of the Ge crystal and the EHD is focused onto an infrared sensitive vidicon tube[44] by means of a high-resolution lens. A silicon filter is employed to remove spurious pumping light. In addition a narrow-band interference filter at 1.75 μm was used to confirm that the detected radiation was recombination luminescence from the electron-hole drop. The electronically scanned image from the vidicon is

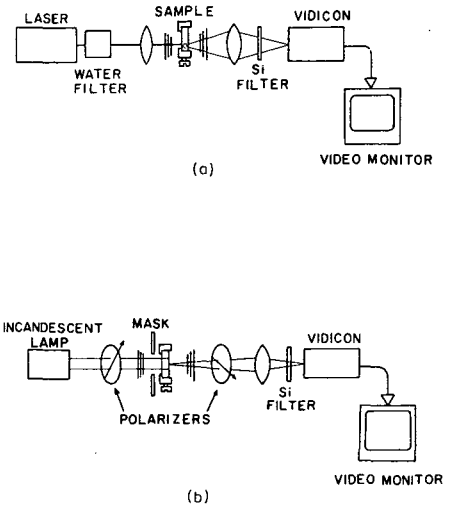

FIG. 18. (a) Arrangement for recording an image of the spatial distribution of the recombination luminescence from the *e-h* liquid in Ge. (b) Arrangement for recording birefringence patterns in strained Ge.

displayed on a standard video monitor cathode ray tube and photographed. The large-drop luminescence spectra were also studied[25]; the spectra are shifted in wavelength due to stress at the center of the well.

Birefringence patterns of the strained sample are obtained using the same image tube, Fig. 18(b). In this case infrared light from a tungsten lamp is linearly polarized and passed through the Ge sample and a second linear polarizer. The variation in index of refraction across the sample gives rise to the strain patterns. It is necessary to mask around the sample to prevent stray light from reaching the vidicon. Thus the birefringence pictures often do not show the entire cross section of the sample. It was possible to simultaneously illuminate the crystal with both the laser and the tungsten lamp, permitting direct comparison of the drop luminescence and the strain pattern.

VII. EXPERIMENTAL RESULTS AND INTERPRETATION

Birefringence patterns for increasing values of applied stress are shown in Fig. 19. The sample is a 4-mm-diam disk with (001) face and a flat on the bottom for edge viewing. The stress is applied along the ⟨110⟩ direction, corresponding to the theoretical graphs of Fig. 14(a). As the force on the plunger is increased a series of dark fringes appears defining surfaces of constant $\epsilon_{zz} - \epsilon_{yy}$ shear strain component as discussed in Sec. IV. The fringes define a point of maximum shear strain inside the sample away from the contacted surface. These data were taken for a crystal temperature

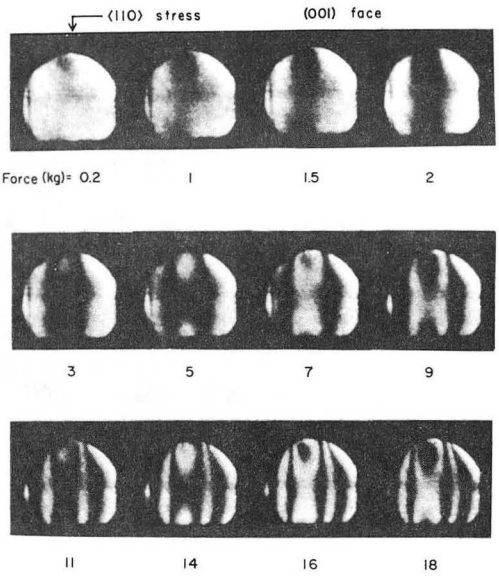

FIG. 19. Birefringence patterns observed in a disk of Ge, for a series of increasing values of applied force on a nylon plunger of contact area ~ 1 mm^2.

of 2 K; however, the intensity of the light from the incandescent lamp is too low to produce an observable electron-hole drop.

When a laser beam is focused onto this sample (power absorbed $\approx$8 mW) an electron-hole drop is formed in the potential well as shown in Fig. 20. The birefringence pattern for this stress, $\approx$9 kg/mm^2 is also shown, as well as the image produced when both the laser and the tungsten lamp illuminate the crystal simultaneously. It can be clearly seen from this photograph that a large EHD is formed at the point of maximum shear stress, as determined by the dark interference fringe. In this experiment the laser was focused to a point nearest the stress maximum; however, the position of the electron-hole drop is unchanged

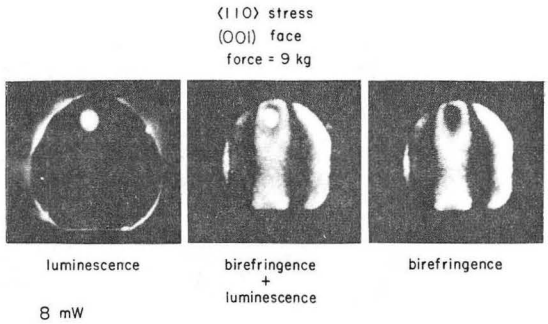

FIG. 20. Luminescence and birefringence patterns observed from Ge stressed along a ⟨110⟩ direction, viewed through an (001) face. In this and subsequent figures the power in mW is the actual power absorbed into the crystal, and the He bath temperature $T \approx 2$ K.

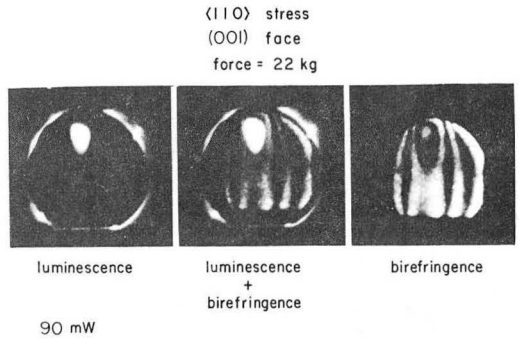

FIG. 21. Luminescence and birefringence patterns in the same sample as Fig. 20, observed at higher pumping intensity and higher stress.

by translating the laser spot. The intensity and size of the luminescent EHD image is reduced somewhat as the laser excitation point is translated away from the stress maximum but the drop is clearly observable even when the laser is focused near the bottom edge of the crystal. The data show that the excitonic matter (carriers, excitons, or small drops) produced at the point of light excitation eventually reach the point of maximum stress where they coalesce into a single large drop.

The size and intensity of the EHD image is dependent upon the laser power. Figure 21(a) shows a larger EHD for an absorbed laser power $\approx$90 mW. In this figure the stress was also increased to 22 kg/mm^2. At this high excitation level it is clear that the electron-hole liquid takes on the asymmetric shape of the strain well. Although surface tension is crucial in the determination of the size and shape of small α-phase droplets in unstressed Ge, in the large drop here the bulk strain forces in the potential well exceed the surface tension by several orders of magnitude. The resulting shape

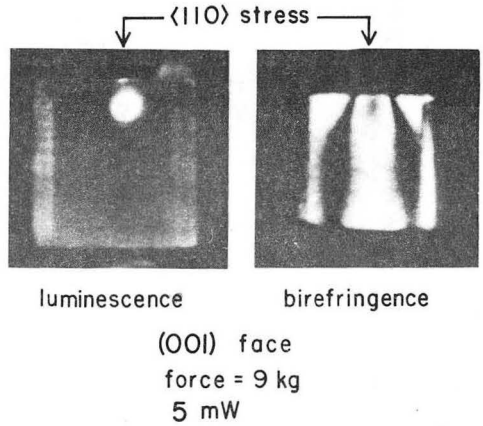

FIG. 22. Luminescence and birefringence patterns in stressed Ge: square sample, $4\times4\times2$ mm^3.

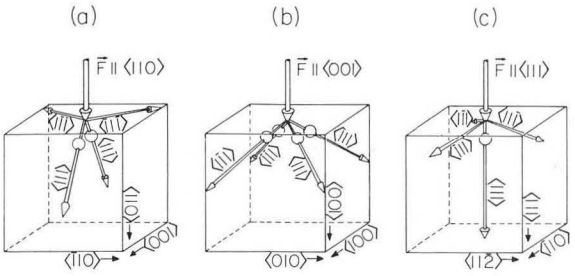

FIG. 23. (a) Location of EHL energy minima in Ge stressed along ⟨110⟩. Greatest energy lowering lies along those two ⟨111⟩ axes whose directions are closest to the direction of applied stress. Solid spheres represent large EHD located at the potential minima. (b) Minima in Ge stressed along ⟨001⟩. All four ⟨111⟩ axes make the same angle with respect to the applied force; thus four minima and four drops are produced. (c) Single minimum produced in Ge stressed along ⟨111⟩.

of this EHD is similar to the theoretical contours of Fig. 11.

Figure 22 shows EHD luminescence and birefringence for a square sample, to be compared with the theoretical contours of Figs. 10(a) and 14(a).

As discussed in Sec. V, the highly anisotropic elastic properties of Ge can give rise to more than one shear stress maximum below the contact area. A shear stress along the crystalline ⟨111⟩ axes

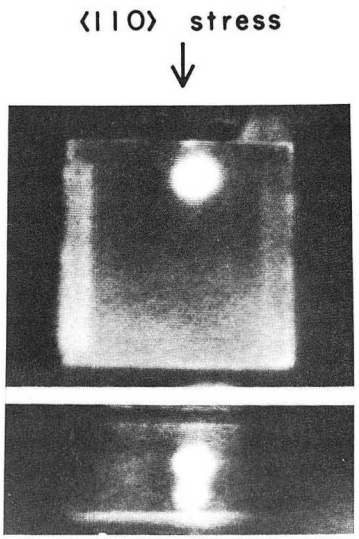

FIG. 24. Luminescence from Ge crystal stressed along a ⟨110⟩ direction, viewed through an (001) face. Lower photo is an end-view through a (110) face and reveals the presence of two EHD in the crystal. Crystal face pumped by the laser beam is shown uppermost in this and the following end-views.

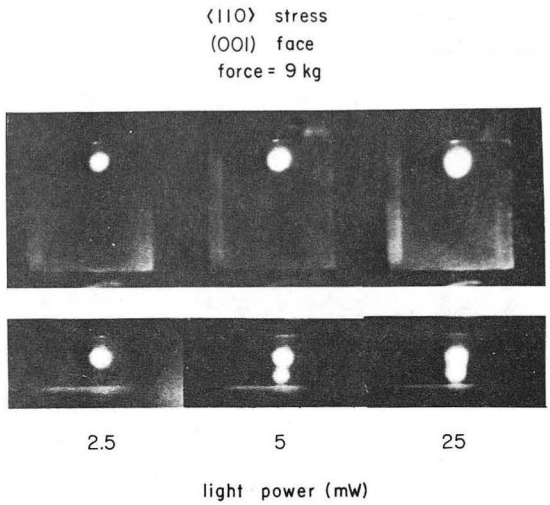

FIG. 25. Luminescence observed from stressed Ge, taken at a series of increasing laser powers. Both potential wells become occupied at higher excitation levels.

produces the largest drop energy lowering, Fig. 4. For stress applied normal to a (110) face the greatest band-edge lowering occurs along the two ⟨111⟩ axes pointing away from the contact point into the crystal at $\theta \approx \pm 35.3°$, as illustrated in Fig. 23(a). Thus two spatially separate potential wells are expected for Ge stressed along ⟨110⟩. If the sample is being viewed through an (001) face, which was the case in the above experiments, one well is located behind the other. A bottom view of the drop luminescence, Fig. 24, shows that this is indeed the case: two distinct drops are produced beneath the stressed surface.

The relative population of the two potential wells, i.e., the size of the two EHD, depends upon the positioning of the laser spot as well as the excitation level. Figure 25 shows that at lower excitation levels, only one of the wells is populated with electron-hole liquid, in this case the well nearer the excitation surface. At higher levels two drops of comparable size are formed.

The existence of multiple potential wells is also observed in the birefringence since the amount of

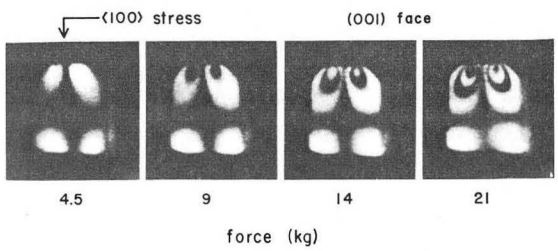

FIG. 26. Birefringence patterns observed from Ge crystal stressed along a ⟨100⟩ direction, viewed through an (001) face.

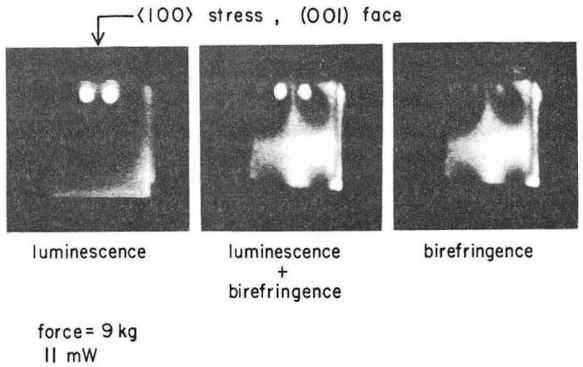

FIG. 27. Luminescence and birefringence patterns observed from Ge stressed along a ⟨100⟩ direction, viewed through an (001) face.

conduction-band lowering determines the change in refractive index. Figure 26 shows the birefringence pattern for a square sample stressed along a ⟨100⟩ direction and viewed through an (001) face. Two strain maxima are visible beneath the contact area precisely as predicted from the two-dimensional analysis of Fig. 14(b). Figure 27 shows a comparison between the drop luminescence and birefringence for this geometry. Of course, the birefringence viewed through the equivalent (010) face must be identical, indicating that there are

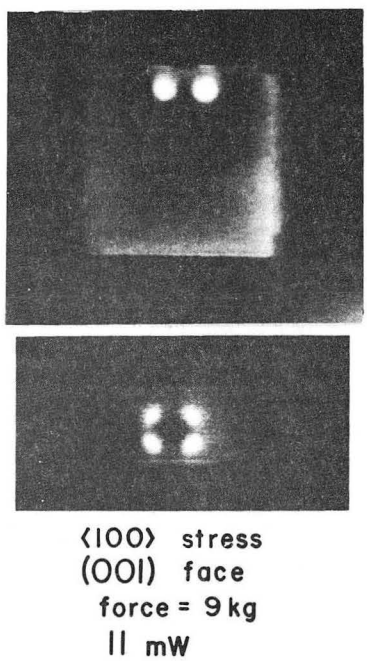

FIG. 28. Luminescence from Ge crystal stressed along a ⟨100⟩ direction, viewed through an (001) face (upper photo), and a (100) face (lower photo). Four drops are formed in this geometry.

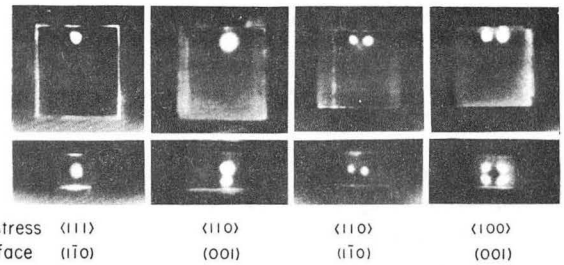

FIG. 29. Luminescence from stressed Ge: summary of four stressing geometries, all at absorbed laser power ~10 mW. Number and position of the drops agree with the theory of Sec. IV; see Fig. 23.

actually four potential wells corresponding to the four ⟨111⟩ directions shown in Fig. 23(b). The luminescence data of Fig. 28 show that indeed four drops are formed in this geometry. Each drop is populated by electrons from only one of the ellipsoids shown in Fig. 2; there is a one-to-one correspondence between the drops in coordinate space and the energy ellipsoids in momentum space.

It is also possible to form a single potential well within the crystal by stressing along a ⟨111⟩ axis, Fig. 23(c). This experiment is shown in Fig. 29, along with a summary of other stress orientations we have tried. In all of these experiments, the number of drops and their location in the crystal agree well with the theory presented in Secs. IV and V.

VIII. DISCUSSION

In this paper we have quantitatively examined a method for confining large volumes of electron-hole liquid. Despite the overall inhomogeneity of the strain distribution within the crystal, the liquid collects in regions of rather well-defined strain conditions, i.e., regions where a single conduction-band minimum is populated (a local ⟨111⟩ shear strain). This corresponds to the configuration Ge(1 : 2) or, at sufficiently high stress, Ge(1 : 1). That is, for all directions of applied stress, even though the number of drops produced may differ, the physical properties of the resulting EHL are always similar. For example, very similar values of EHL lifetime have been obtained for ⟨111⟩, ⟨110⟩, and ⟨100⟩ stressed samples: we find $\tau \approx 300$ to 600 μsec at 1.8 K, compared with 40 μsec for Ge(4 : 2). Since the EHL lifetime is directly dependent on drop density, which should be sensitive to the configuration of the Ge,[9,17] we conclude that these various stress geometries correspond to the same configuration, most likely Ge(1 : 2).

We observe that the initial decay rate is higher

for larger drops. This may be due to a radial variation of pair density produced by compression of the drop in the strain gradient; this will be discussed more fully in Ref. 25.

The volume of the confined electron-hole liquid is considerably larger than the total volume of electron-hole droplets produced in unstressed Ge. This is because the lifetime is about an order of magnitude larger and the density three to four times smaller than for Ge(4 : 2). Thus for a given production efficiency (photons to e-h pairs in EHL), the volume would be perhaps 30 to 40 times larger in the strained case. This factor becomes even larger at 4.2 K, where evaporation from the small α drops in unstrained Ge greatly reduces the liquid volume. The production efficiency may not be the same for the α and γ phases, however. Surface conditions, strain geometry, and excitation conditions all can influence production efficiency. For instance, we find that the volume of liquid is somewhat reduced for an unfocused laser beam or for a laser spot focused far from the stress maximum. An experimental comparison of the properties of the α and γ phases will be reported separately.[25]

In order to have a high production efficiency for the γ phase, it is necessary that the γ drops form in a time short compared with the exciton or α-phase lifetime. Alfvén wave resonances[45] have been used to measure formation times of 1 to 2 μsec for large EHD after a 100 nsec light pulse. These short times are consistent with transit times of carriers from the crystal surface to the position of minimum energy, using the strain gradients produced under our stress conditions.

In summary, we have been able to produce large drops of electron-hole liquid in a stable and reproducible manner. Using such large drops, it is possible to probe the interior of an EHD, with experiments such as Alfvén wave resonance,[27] ultrasonic attenuation,[30] and far-infrared absorption.[46] These and related experiments give further insight into the properties of the electron-hole liquid.

ACKNOWLEDGMENTS

We would like to thank R. L. Taylor, T. J. R. Hughes, W. Kanoknukulchai, and A. Curnier for kindly allowing us to use their general finite element analysis programs and for their assistance. We thank W. L. Hansen and E. E. Haller for providing us with the ultrapure Ge samples and the infrared vidicon. We gratefully acknowledge many useful discussions with C. Kittel. One of the authors (R.S.M.) would like to thank IBM for the support provided through a Postdoctoral Fellowship.

APPENDIX: OCTAHEDRAL SHEAR STRAIN

The shear strains

$$\epsilon_0^i = \hat{a}_i \cdot \vec{\epsilon} \cdot \hat{a}_i - \tfrac{1}{3}\,\mathrm{Tr}\vec{\epsilon} \tag{A1}$$

play an important role in the study of EHL energy lowering, as can be seen from Eq. (5). Since each strain is associated with a particular ⟨111⟩ axis, they could be called octahedral shear strains.[47] However, we reserve that name for $\epsilon_0^m = \max(-\epsilon_0^i)$, which is generally the largest magnitude of any ϵ_0^i (compressional strains are taken to be negative).

These ϵ_0^i may always be defined in terms of a ⟨100⟩ coordinate system. Thus if $\hat{a}_i = (1/\sqrt{3})(l,m,n)$, where $l, m, n = \pm 1$, we have

$$\epsilon_0^i = \tfrac{2}{3}(\epsilon_{12} lm + \epsilon_{13} ln + \epsilon_{23} mn). \tag{A2}$$

For a two-dimensional case ($\epsilon_{11} = \epsilon_{12} = \epsilon_{13} = 0$), we have

$$\epsilon_0^m = -\tfrac{2}{3}\epsilon_{23}. \tag{A3}$$

However, it is usually more convenient to define ϵ_0^i in terms of the x, y, and z axes, with the force applied along the z axis, and the crystal face in the y-z plane. Thus, for example, if the stress is applied in the ⟨110⟩ direction to a crystal whose face is in a (001) plane,

$$\epsilon_0^m = \tfrac{1}{3}(\epsilon_{yy} - \epsilon_{zz}). \tag{A4}$$

We may define stress components σ_0^i accordingly:

$$\sigma_0^i = \hat{a}_i \cdot \vec{\sigma} \cdot \hat{a}_i - \tfrac{1}{3}\,\mathrm{Tr}\vec{\sigma}, \tag{A5}$$

with $\sigma_0^m = \max_i(-\sigma_0^i)$. Whereas, in general, components of $\vec{\sigma}$ and $\vec{\epsilon}$ are related via a tensor $\underline{C}$, the σ_0^i and ϵ_0^i are related by a scalar. In a ⟨1$\bar{1}$0⟩ coordinate system, with $\hat{a}_i = (1/\sqrt{3})(l,m,n)$:

$$\begin{aligned}\sigma_0^i &= \tfrac{2}{3}(lm\sigma_{12} + ln\sigma_{13} + mn\sigma_{23}) \\ &= C_{44}\tfrac{2}{3}(lm\epsilon_{12} + ln\epsilon_{13} + mn\epsilon_{23})\end{aligned}$$

or

$$\sigma_0^i = C_{44}\epsilon_0^i. \tag{A6}$$

Finally, it was noted in the text that the birefringence pattern is usually proportional to ϵ_0^m. This can be shown to hold in general, if the strain-optic tensor $\underline{p}$ [Eq. (12)] has the property that $p_{11} = p_{12}$ (as is approximately true for Ge). The dielectric constant tensor is

$$\vec{\kappa} = \kappa_L \vec{I} + \vec{\kappa}',$$

$$\vec{\kappa}' = \kappa_L^2\, \underline{p} : \vec{\kappa},$$

where $\vec{I}$ is a unit tensor. When $p_{11} = p_{12}$, we have

$$\kappa'_{11} = p_{11}\epsilon_{11} + p_{12}(\epsilon_{22}+\epsilon_{33}) = p_{11}\,\mathrm{Tr}\bar{\bar{\epsilon}}\,,$$

or

$$\bar{\bar{\kappa}}' = \kappa_L^2\left[p_{11}(\mathrm{Tr}\bar{\bar{\epsilon}})\bar{\bar{I}} + p_{44}\begin{pmatrix} 0 & \epsilon_{12} & \epsilon_{13} \\ \epsilon_{12} & 0 & \epsilon_{23} \\ \epsilon_{13} & \epsilon_{23} & 0 \end{pmatrix}\right]. \quad \text{(A7)}$$

Terms proportional to the identity matrix cannot contribute to the birefringence; thus the important components of $\bar{\bar{\kappa}}'$ are proportional to just those components of $\bar{\bar{\epsilon}}$ which determine the ϵ_0^i [Eq. (A2)]. If $\epsilon_0^m = -\epsilon_0^{i'}$, then by aligning the axes of the polarizers along or perpendicular to $\hat{a}_{i'}$, the birefringence fringe order N will be approximately proportional to ϵ_0^m.

Note added in proof. It now appears that the long lifetime (500 μsec) we report here for γ drops is only observed in dislocation-free samples of Ge. In dislocated specimens we observe a short lifetime (~40 μsec) for γ drops. Ya. Pokrovskii [Proceedings of the Thirteenth International Conference on Physics of Semiconductors, Rome, Aug. 30–Sept. 3, 1976 (unpublished)] has recently reported a long lifetime (~300 μsec) for the electron-hole drops in uniaxially stressed dislocation-free Ge.

---

*Supported in part by U. S. ERDA.

†Present address: Physics Dept., Univ. of Illinois, Urbana, Illinois 61801.

[1]L. V. Keldysh, in *Proceedings of the Ninth International Conference on Physics of Semiconductors, Moscow* (Nauka, Leningrad, 1968), p. 1303.

[2]For reviews see Ya. Pokrovskii, Phys. Status Solidi A 11, 385 (1972); C. D. Jeffries, Science 189, 955 (1975); W. F. Brinkman, J. C. Hensel, T. G. Phillips, and T. M. Rice, Solid State Phys. (to be published).

[3]Ya. E. Pokrovskii and K. I. Svistunova, Zh. Eksp. Teor. Fiz. Pis'ma Red. 13, 297 (1971) [JETP Lett. 13, 212 (1971)].

[4]J. M. Worlock, T. C. Damen, K. L. Shaklee, and J. P. Gordon, Phys. Rev. Lett. 33, 771 (1974).

[5]Ya. E. Pokrovskii and K. I. Svistunova, Fiz. Tekh. Poluprovadn. 4, 491 (1970) [Sov. Phys.-Semicond. 4, 409 (1970)].

[6]C. Benoit à la Guillaume, M. Voos, and F. Salvan, Phys. Rev. B 5, 3079 (1972).

[7]G. A. Thomas, T. M. Rice, and J. C. Hensel, Phys. Rev. Lett. 33, 219 (1974).

[8]M. Combescot, Phys. Rev. Lett. 32, 15 (1974); M. Droz and M. Combescot, Phys. Lett. A 51, 473 (1975).

[9]P. Vashishta, S. G. Das, and K. S. Singwi, Phys. Rev. Lett. 33, 911 (1974).

[10]T. L. Reinecke and S. C. Ying, Phys. Rev. Lett. 35, 311 (1975).

[11]T. K. Lo, B. Feldman, and C. D. Jeffries, Phys. Rev. Lett. 31, 224 (1973).

[12]R. M. Westervelt, J. L. Staehli, E. E. Haller, and C. D. Jeffries, in *Lecture Notes in Physics*, Vol. 57, edited by M. Ueta and Y. Nishina (Springer-Verlag, Heidelberg, 1976), p. 270; R. M. Westervelt, Phys. Status Solidi B 74, 727 (1976); R. M. Westervelt, Phys. Status Solidi B 76, 31 (1976); R. M. Westervelt, J. L. Staehli, and E. E. Haller (unpublished).

[13]W. F. Brinkman, T. M. Rice, P. W. Anderson, and S. T. Chui, Phys. Rev. Lett. 28, 961 (1972); W. F. Brinkman and T. M. Rice, Phys. Rev. B 7, 1508 (1973).

[14]M. Combescot and P. Nozières, J. Phys. C 5, 2369 (1972).

[15]P. Vashishta, P. Bhattacharyya, and K. S. Singwi, Phys. Rev. B 10, 5108 (1974); P. Bhattacharyya, V. Massida, K. S. Singwi, and P. Vashishta, *ibid.* 10, 5127 (1974).

[16]The notation Ge(i:j) refers to the number of conduction-band minima (i) and valence-band maxima (j) occupied in the liquid phase. Thus Ge(4:2) refers to unstressed germanium (see Fig. 3).

[17]P. Vashishta, R. K. Kalia, and K. S. Singwi, in *Lecture Notes in Physics*, Vol. 57, edited by M. Ueta and Y. Nishina (Springer-Verlag, Heidelberg, 1976), p. 187.

[18]V. S. Bagaev, T. I. Galkina, O. V. Gogolin, and L. V. Keldysh, Zh. Eksp. Teor. Fiz. Pis'ma Red. 10, 309 (1969) [Sov. Phys-JETP Lett. 10, 195 (1969)]. Motion of EHD in a strain gradient with velocities $v \approx 3 \times 10^5$ cm/sec was reported by A. S. Alekseev, T. A. Astimerov, V. S. Bagaev, T. I. Galkina, N. A. Penin, N. N. Sybeldin, and V. A. Tsvetkov, in *Proceedings of the Twelfth International Conference on Physics of Semiconductors*, edited by M. H. Pilkuhn (Teubner, Stuttgart, 1974), p. 91.

[19]J. C. Hensel, T. G. Phillips, and T. M. Rice, Phys. Rev. Lett. 30, 227 (1973).

[20]R. M. Westervelt, T. K. Lo, J. L. Staehli, and C. D. Jeffries, Phys. Rev. Lett. 32, 1051 (1974); 34, 1331 (E) (1974).

[21]A. S. Alekseev, V. S. Bagaev, and T. I. Galkina, Zh. Eksp. Teor. Fiz. 63, 1020 (1972) [Sov. Phys.-JETP 36, 536 (1973)].

[22]H. Hertz, J. Math. (Crelle's J.) 92, 156 (1881).

[23]J. P. Wolfe, W. L. Hansen, E. E. Haller, R. S. Markiewicz, C. Kittel, and C. D. Jeffries, Phys. Rev. Lett. 34, 1292 (1975); J. P. Wolfe, R. S. Markiewicz, and C. D. Jeffries, in *Proceedings of the Third International Conference on Light Scattering in Solids, Campinas*, edited by R. C. C. Leite (Flammarion, Paris, 1975), p. 173. R. S. Markiewicz, thesis (University of California, Berkeley, 1975) (unpublished).

[24]J. P. Wolfe, R. S. Markiewicz, C. Kittel, and C. D. Jeffries, Phys. Rev. Lett. 34, 275 (1975).

[25]J. P. Wolfe *et al.* (unpublished).

[26]M. Voos, K. L. Shaklee, and T. M. Worlock, Phys. Rev. Lett. 33, 1161 (1974); R. W. Martin, thesis (Stuttgart, 1974) (unpublished).

[27]R. S. Markiewicz, J. P. Wolfe, and C. D. Jeffries, Phys. Rev. Lett. 32, 1357 (1974); 34, 59 (E) (1975). The existence of large EHD was first inferred from these microwave magnetoplasma dimensional reson-

ances. It was later found (Ref. 24) that the original sample holder fortuitously introduced a strain potential well. See also R. S. Markiewicz, thesis, Ref. 23.

[28]C. D. Jeffries, J. P. Wolfe, S. M. Kelso, R. S. Markiewicz, and J. E. Furneaux, J. of Lumin. 12, 659 (1976).

[29]Ya. E. Pokrovskii and K. I. Svistunova, Zh. Eksp. Teor. Fiz. Pis'ma Red. 23, 110 (1976).

[30]T. Ohyama, A. D. A. Hansen, and J. L. Turney, Solid State Commun. 19, 1083 (1976).

[31]C. Herring and E. Vogt, Phys. Rev. 101, 944 (1956).

[32]G. E. Picus and G. L. Bir, Fiz. Tverd. Tela 1, 1642 (1959) [Sov. Phys.-Solid State 1, 1502 (1959)].

[33]I. Balslev, Phys. Rev. 143, 636 (1966).

[34]For reviews of the contact problem, see, for example, S. P. Timoshenko and J. N. Goodier, *Theory of Elasticity*, 3rd ed. (McGraw-Hill, New York, 1970), Chap. 12; and R. C. Juvinall, *Engineering Considerations of Stress, Strain, and Strength* (McGraw-Hill, New York, 1967), Chap. 18.

[35]M. T. Huber, Ann. Phys. (Paris) 14, 153 (1904); S. Fuchs, Phys. Z. 14, 1282 (1913); M. T. Huber and S. Fuchs, Phys. Z. 15, 298 (1914).

[36]As explained in the text, we use the room-temperature elastic constants: for Ge, $C_{11}=1.285\times10^{12}$ dyn/cm^2, $C_{12}=0.483\times10^{12}$, $C_{44}=1.36\times10^{12}$ [C. Kittel, *Introduction to Solid State Physics*, 4th ed. (Wiley, New York, 1971), Chap. 4]; for nylon, the stiffness tensor was determined from Young's modulus $Y=3.58\times10^{10}$ dyn/cm^2, and Poisson's ratio $\nu=0.4$ [*American Institute of Physics Handbook*, 2nd ed. (McGraw-Hill, New York, 1963), Table 3*f*-2]. At liquid-He temperatures $Y\sim9.2\times10^{10}$ dyn/cm^2 [J. M. Crissman, J. A. Sauer, and A. E. Woodward, J. Polym. Sci. A 2, 5075 (1964)].

[37]For large z, σ_{yy} has a small but nonzero negative value. The true value at the Ge-quartz interface is probably smaller, and depends on the amount of sticking between the different materials. *For this surface*, the calculation was simplified by assuming perfect sticking.

[38]T. J. R. Hughes, R. L. Taylor, J. L. Sackman, A. Curnier, and W. Kanoknukulchai, J. Comp. Meth. Appl. Mech. Eng. 8, 249 (1976); O. C. Zienkiewicz, *The Finite Element Method in Engineering Science* (McGraw-Hill, New York, 1971).

[39]We considered two limits of the two-dimensional elastic problem: the third dimension can either be considered infinitely long (known as the plane strain problem) or infinitessimally thick (plane stress). Both problems were solved and the differences in strain distribution were found to be small. The results in the text and figures are given for the plane stress problem.

[40]R. S. Leigh and B. Szigeti, Proc. R. Soc. A 301, 211 (1967).

[41]This result is true in three dimensions only if Poisson's ratio $\nu=0.5$; otherwise there are additional terms in the stress tensor proportional to $(1-2\nu)$. An analogous result holds in two dimensions, $\sigma\propto r^{-1}\cos\theta$. See Timoshenko, Ref. 34, Eqs. (65) and (211).

[42]W. L. Hansen and E. E. Haller, IEEE Trans. Nucl. Sci. 21, 251 (1974).

[43]Vespel is a high strength polymer with a low thermal expansion, kindly supplied by Dr. H. Jarrett.

[44]Type N214 manufactured by Hamamatsu Corporation.

[45]J. E. Furneaux, J. P. Wolfe, and C. D. Jeffries, Solid State Commun. 20, 317 (1976).

[46]R. L. Aurbach, L. Eaves, R. S. Markiewicz, and P. L. Richards, Solid State Commun. 19, 1023 (1976).

[47]This is not the same as the octahedral shearing stress and strain introduced in plasticity theory: see Y. C. Fung, *Foundations of Solid Mechanics* (Prentice-Hall, Englewood Cliffs, N. J., 1965), p. 81.

TECHNICAL INFORMATION DIVISION
LAWRENCE BERKELEY LABORATORY
UNIVERSITY OF CALIFORNIA
BERKELEY, CALIFORNIA 94720